Mon. Not. R. Astron. Soc. 293, 189–196 (1998)

Near-infrared line and radio continuum imaging of the Circinus galaxy

Richard I. Davies,[1]★ Duncan A. Forbes,[2] Stuart Ryder,[3]† Michael C. B. Ashley,[3] Michael Burton,[3] John W. V. Storey,[3] Lori E. Allen,[3] Martin J. Ward[4] and Ray P. Norris[5]

[1]*Astrophysics, Nuclear Physics Building, Keble Road, Oxford OX1 3RH*
[2]*School of Physics and Space Research, University of Birmingham, Edgbaston, Birmingham B15 2TT*
[3]*School of Physics, University of New South Wales, Sydney 2052, Australia*
[4]*Department of Physics and Astronomy, Leicester University, Leicester LE1 7RH*
[5]*Australia Telescope National Facility, CSIRO Radiophysics Laboratory, PO Box 76, Epping NSW 2121, Australia*

Accepted 1997 September 9. Received 1997 August 11; in original form 1997 February 26

ABSTRACT

We have imaged the Circinus galaxy in the near-infrared [Fe II] 1.64-μm and H_2 2.12-μm lines, and derived velocity maps for the emission. The morphologies are strikingly different, but the velocity maps are very similar and consistent with simple rotation. We also present new radio continuum maps at 3 and 6 cm, which show a partially resolved nucleus with a flat spectral index. This suggests free–free absorption rather than self-absorption in a compact source. There is some evidence of radio jets close to the nucleus. The H_2 emission, rather than the [Fe II] as in NGC 1068, is extended along the jet axis and may be excited by jet-induced shocks either in a low-density medium or with rather slow shock speeds ($v \lesssim 50$ km s^{-1}). We find that the star formation in the ring 10 arcsec from the nucleus began less than a few $\times 10^7$ yr ago. Nearer the AGN, perhaps in and around the inferred torus, we detect extended [Fe II] emission (including one prominent peak about 2 arcsec north of the AGN which could be due to a single young remnant), from which we derive a modest star formation rate of < 1 M$_\odot$ yr^{-1}.

Key words: galaxies: individual: Circinus – galaxies: Seyfert – infrared: galaxies – radio continuum: galaxies.

1 INTRODUCTION

The Circinus galaxy was first studied by Freeman et al. (1977). Although it lies within a few degrees of the Galactic plane, it is seen through a low-extinction window and therefore can be studied at optical wavelengths, appearing as a spiral galaxy with an intrinsic dust lane, inclined at about 65° (Freeman et al. 1977). These authors derived a distance of 4 Mpc from the observed recessional velocity of 436 km s^{-1} (correcting for the velocity of the Local Group and using $H_0 = 50$ km s^{-1} Mpc^{-1}), as well as from other measures. Their optical spectroscopy showed it to have very strong emission lines of [O III] and H α. More recently, the detection of high-ionization coronal lines in the optical and infrared confirm the Circinus galaxy as a type 2 Seyfert (Oliva et al. 1994), thereby making it the nearest active galactic nucleus (AGN). Recent mid-infrared spectroscopy with *ISO* has revealed evidence suggestive of photoionization by both starbursts and AGN (Moorwood et al. 1996). Emission-line images have also revealed a remarkable ionization cone originating at the nucleus and a circumnuclear ring of star formation about 10 arcsec away (Marconi et al. 1994). Uncalibrated line-maps of prominent near-infrared lines (Moorwood & Oliva 1994) showed strong nuclear peaks, and that while both [Fe II] and H_2 had continuous extended emission, the Br γ was more ring-like. Other indications of intense activity in this galaxy include observations of powerful and rapidly variable H_2O masers (Gardner & Whiteoak 1982; Whiteoak & Gardner 1986; Greenhill et al. 1997).

The nucleus of Circinus has also been the subject of *ASCA* observations in the 2–10 keV band (Matt et al. 1996). These show that the X-ray spectrum has a flat continuum and a prominent Fe 6.4-keV line, which are interpreted as a reflection-dominated spectrum, perhaps cold matter illumi-

★E-mail: rid@astro.ox.ac.uk (RID)
†Present address: Joint Astronomy Centre, 660 North A'ohōkū Place, Hilo, HI 96720, USA.

nated by an obscured AGN. The more extended regions have been mapped by radio continuum observations (Harnett et al. 1990), which revealed two spurs of emission roughly aligned with the minor axis of the galaxy (PA $= -60°$). OH observations by the same authors showed there to be rotation with a total spread of 180 km s^{-1} in the central 12.5 arcmin, consistent with ± 118 km s^{-1} for the H I line measured by Freeman et al. (1977) in the flat part (15–32 arcmin) of the rotation curve. Further radio continuum observations (Elmouttie et al. 1995) have shown that the radio lobes are polarized by up to 45 per cent.

The inner regions of active galaxies are often highly obscured, and thus the near-infrared lines are well suited to studying these objects, since $A_K \sim 0.1\, A_V$. We present here high-resolution images of two such prominent lines, [Fe II] 1.64 μm and H_2 1–0S(1) 2.12 μm, which are associated with both AGN and star formation activity. The instrument used was the newly commissioned University of New South Wales Infrared Fabry–Perot (UNSWIRF), which has a resolving power equivalent to a velocity resolution of 70 km s^{-1}, allowing the relative velocity of the emission lines to be mapped, and providing information about the dynamics of the excited gas. Radio continuum maps at 3 and 6 cm complement the line images, and enhance the interpretation, allowing us to distinguish free–free and synchrotron processes.

2 OBSERVATIONS AND DATA REDUCTION

UNSWIRF is a 70-mm-diameter Queensgate (UK) Ltd. etalon with $R \sim 4000$, tunable over both the H and K windows. When used in conjunction with the wide-field mode of the infrared imager/spectrograph IRIS (Allen et al. 1993), which uses a 128×128 HgCdTe array at the $f/36$ focus of the Anglo-Australian Telescope, a (roughly circular) field of 1.7-arcmin diameter at 0.77 arcsec pixel^{-1} is produced. Appropriate 1 per cent bandpass filters are used to ensure that only a single order is passed by the etalon.

Observations of Circinus in the H_2 1–0S(1) (2.12-μm) and [Fe II] (1.64-μm) lines were obtained on 1996 April 5 UT. The Brγ (2.17-μm) line was not observed due to time and weather constraints. The etalon spacing was determined after calibrating on the peak of the 2.12-μm H_2 line in OMC-1 and then offsetting for the appropriate redshift (436 km s^{-1}) for the source. A sequence of seven images spanning the peak of the 2.12-μm line and separated by ~ 1.2 times the instrumental profile width were obtained, and similarly for the 1.64-μm line. In each case, another image at 8–9 profile widths from the line centre was obtained in order to sample the continuum. An integration time of 120 s per etalon setting was used, with non-destructive readouts every 5 s. The same exposure sequence was carried out on the sky 5 arcmin east of Circinus. Most of the object and sky exposures were repeated (with slight offsets from the previous positions), leading to total on-source integration times of 1440 and 1200 s in the 2.12 and 1.64-μm lines respectively.

Dark-current subtraction and linearization are performed during readout. The object frames were sky-subtracted, and then flat-fielded using normalized dome flat-fields, using in each case images at the matching etalon settings. The frames were then registered using field stars, and all frames at a given etalon setting were averaged together. The continuum frames, appropriately scaled, were then subtracted from all other images to leave just pure line emission in each.

At this stage, the emission-line images were 'stacked' into cubes of increasing etalon spacing (wavelength) so that a Lorentzian profile could be fitted to the 7-point spectrum at each pixel. Having already fixed the continuum level to be zero, the number of free parameters in the fitting was further reduced by constraining the width of the profile to be the same as that found by fits to high-resolution scans of arc lines (Kr 2.1165 μm and Ar 1.6436 μm for the 2.12 and 1.64-μm cubes respectively). The output of the line fitting includes maps of the peak intensity, as well as the etalon setting corresponding to that peak. Blanking masks are constructed by requiring the peak intensity in a given pixel to lie above a user-determined cut-off level, while at the same time the fitted peak position must lie within the range covered by the etalon sequence. Flux calibration, and continuum scaling factors, are provided by photometry of 10×1 s observations of the spectroscopic standard BS 5699 ($K = 4.10$) at the same etalon settings used for Circinus.

The seeing for these observations, as measured from the profile of the standard stars used for calibration, is approximately 1.4 arcsec, close to the resolution limit imposed by the pixel scale of 0.77 arcsec pixel^{-1}. The seeing is shown in Fig. 1 (represented by a circle), although the resolution of these longer exposure frames may be slightly worse than for the stars.

Radio continuum observations of Circinus were carried out using the Australia Telescope Compact Array (ATCA) on 1994 November 14. Data were obtained at 4.79 GHz (6 cm) and 8.64 GHz (3 cm) simultaneously. The half-power beam-widths of the final maps are 1.92×1.64 arcsec^2 at PA $= -36°$ and 1.06×0.91 arcsec^2 at PA $= -39°$ for the 6- and 3-cm maps respectively. The phase calibrator used was PKS B1236 − 684 (a quasar), and the amplitude calibrator was PKS B1934 − 638 (a radio galaxy). The data were edited, calibrated and CLEANed using AIPS software.

3 RESULTS AND DISCUSSION

3.1 Extinction

Estimating extinction is a difficult issue, as it will vary, probably significantly, across the object, and so any measurement on the nucleus will not necessarily be representative of the average value. The Galactic extinction is $A_V = 1.5$ mag (Freeman et al. 1977), but at the nucleus Marconi et al. (1994) argue that an apparent shift between peaks in different bands is due to $A_V \approx 20$ mag, consistent with that derived from mid-infrared observations (Moorwood & Glass 1984). Matt et al. (1996) use a column density of $N_H = 3 \times 10^{21}$ cm^{-2} when modelling the X-ray emission, although they note that for the nucleus to be obscured up to 10 keV the column density should be at least 10^{24} cm^{-2}, equivalent to $A_V \sim 500$ mag (assuming a gas-to-dust ratio of 100). It is reasonable to assume that the [Fe II] and H_2 will be produced much further from the AGN than the X-ray emission, as implied by the marginally resolved central peaks, and so will suffer far less extinction. Even so, there may still be a large extinction that can impose considerable

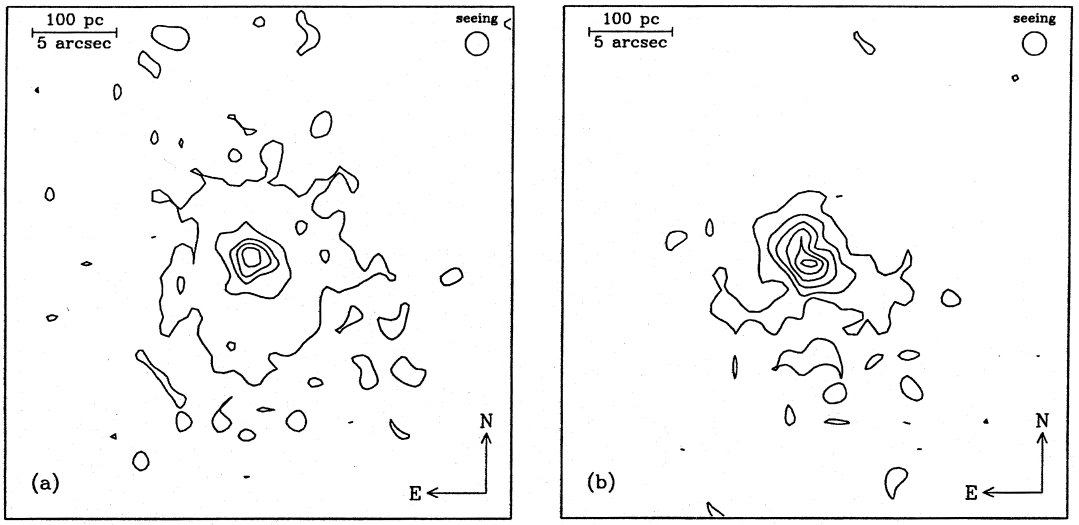

Figure 1. Emission-line images for the central 30×30 arcsec^2. (a) H_2 1–0S(1) 2.12 μm. The single peak is surrounded by a fainter axisymmetric emission. Contours are from 10^{-18} W m^{-2} arcsec^{-2} (2.5σ) to 9×10^{-18} W m^{-2} arcsec^{-2}, at intervals of 2×10^{-18} W m^{-2} arcsec^{-2}. (b) [Fe II] 1.64 μm, clearly showing two peaks. Contours are from 1.25×10^{-18} W m^{-2} arcsec^{-2} (2.5σ) to $7.5 \times 10^{-}$ W m^{-2} arcsec^{-2}, at intervals of 1.25×10^{-18} W m^{-2} arcsec^{-2}. The ionization cone lies towards the north-west, and extends past the circumnuclear ring at a radius of 10 arcsec.

uncertainty on any determination of the intrinsic line ratio. Adopting $A_V = 20$ as discussed above, we find $A_H = 3.5$ and $A_K = 1.6$ (Howarth 1983), so that the dereddened nuclear fluxes are 117×10^{-17} W m^{-2} for [Fe II] and 14×10^{-17} W m^{-2} for 1–0 S(1) (compared to those in Table 1). However, the uncertainty in the extinction means that these fluxes could be different by a large factor, and the fluxes are therefore unreliable. As such, when dereddening the measured fluxes we have only accounted for Galactic absorption, adopting values of $A_H = 0.26$ and $A_K = 0.12$. The fact that the [Fe II] and radio fluxes fit the correlation of Forbes & Ward (1993) using this low extinction (see Section 3.4) tends to support its use. Nevertheless, it is possible that the intrinsic fluxes, especially near the AGN, may be significantly greater.

In Table 1 we report the adopted fluxes (corrected for Galactic extinction). The fluxes in a 6×6 arcsec^2 aperture are approximately 50 per cent more than those measured by Moorwood & Oliva (1988).

Table 1. Line fluxes.

Region/Feature	Flux[c] ($\times 10^{-17}$ W m^{-2})	
	H_2 2.12 μm	[Fe II] 1.64 μm
Nucleus[a]	5.1	5.8
Northern peak[a]	$3\sigma < 0.7$	2.9
Extended emission[b]	43.1	31.5
Total (in 30 arcsec)	48.2	40.2

[a]Fluxes measured by fitting and subtracting Gaussians (see text for details).
[b]In a 30×30 arcsec^2 aperture, after subtracting the point sources.
[c]Corrected for Galactic, but not internal, extinction.
Statistical errors are less than 5 per cent, but the major source of uncertainty is from calibration and point source subtraction.

3.2 H_2 1–0S(1) 2.12 μm

The H_2 emission in Fig. 1(a) shows a single peak (FWHM 2.2 arcsec) that is marginally resolved (seeing is 1.4 arcsec). This is consistent with a molecular torus, the presence of which is inferred from its collimating effect in producing the ionization cone. In Circinus the cone extends some 20 arcsec towards the north-west; the northern edge is sharply defined at PA $= -25°$, while the southern edge opens out at a radius of about 10 arcsec to PA $= -70°$ (Marconi et al. 1994). The geometry of molecular tori is rather uncertain. The inner edge is believed to lie at a radius of about 1 pc (Krolik & Begelman 1988), and there are two different arguments for the position of the outer edge (Krolik & Begelman 1988; Yi, Field & Blackman 1994) which place it at a few to a few tens of parsecs. The maximum extent need not necessarily be well defined if the gas density in the torus decreases slowly, and it is possible that the fainter diffuse emission may be the outer regions of the same structure. Supporting this interpretation is the radial profile of the total H_2 emission, shown in Fig. 2(a), which can be well fitted by a single power law of slope -1.2 for $r > 1$ arcsec. At radii less than this, the power law is no longer valid due to the effects of seeing and the inner edge of the torus. Such a model might be plausible if the H_2 is produced solely by X-ray heating of the molecular gas, but since even the unabsorbed X-ray intensity must decrease as r^{-2}, we expect the H_2 intensity to fall away even more steeply. Further evidence against this is provided by the isobaric model of Lepp & McCray (1983), which predicts an 1–0S(1) luminosity from the 2–10 keV luminosity. Using the *ASCA* flux of 10^{-14} W m^{-2} in this band, we predict an S(1) flux that is an order of magnitude less than the observed total. Accordingly, we decompose the emission as shown in Fig. 2(b) into a central source (which *may* be associated with the AGN)

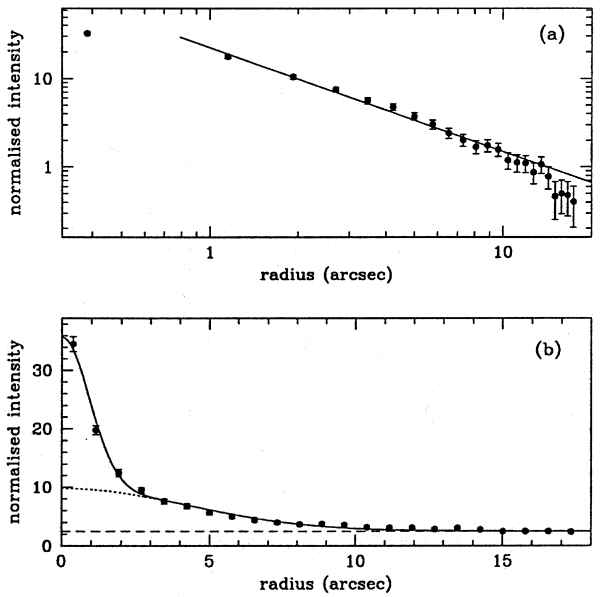

Figure 2. Radial profile of the H_2 emission. (a) A best-fitting power-law model in the region $r = 1$–17 arcsec, where $I \propto r^{-1.2}$. (b) Two Gaussians: a marginally resolved central source (FWHM 2.2 arcsec) superimposed on extended emission (FWHM 10.0 arcsec).

superimposed on an extended region approximated by a Gaussian of FWHM 10.0 arcsec, which is probably excited by star formation or jet-induced shocks. In such a situation it is only the central source (but not necessarily even that) which would be produced by X-ray heating of the H_2, and we find that the predicted 1–0S(1) flux is similar to the observed nuclear source flux in Table 1.

We now consider the circumnuclear star formation which was observed in Hα (Marconi et al. 1994) and in Brγ (uncalibrated; Moorwood & Oliva 1994), but which we have not detected in H_2. Marconi et al. (1994) proposed a simple model in which a wave of star formation is propagating outward to explain observations of late-type stars near the nucleus and young stars in the ring. Assuming this to be the case, the H_2 emission we observe should originate in supernova remnants (SNRs) or stars of a few solar masses left over from a short burst of star formation a few $\times 10^8$ yr previously. Since the progenitors of SNRs are stars of mass > 8 $M_\odot$ with main-sequence lifetimes $< 10^8$ yr, the contribution from such SNRs would increase sharply near the ring. We also consider the B-star contribution using the data for 1–0S(1) line luminosity from Puxley, Hawarden & Mountain (1990). This would increase further from the AGN since, for any reasonable initial mass function (IMF), the more massive (up to at least 8 $M_\odot$) and hence younger stars produce a combined 1–0S(1) luminosity which more than offsets the smaller number of such stars. Any extended emission at the star-forming ring is below our detection threshold of 6×10^{-19} W m^{-2} arcsec^{-2}, although we cannot rule out the possibility that there is weak emission associated with the ring. However, we can rule out the scenario described above, since the observed H_2 emission decreases smoothly further from the AGN, contrary to what is predicted. We conclude that the H_2 emission within 6–7 arcsec of the AGN is due (at least in part) to ongoing star formation, perhaps this and the AGN being fuelled by an inward drift of residual gas from star formation at the ring (e.g. Pfenniger & Norman 1990). This star-forming ring, which has a diameter of 400 pc consistent with that expected for an inner Lindblad resonance (ILR), is a separate phenomenon which may have been triggered dynamically by gas inflow from the disc. A bar-driven inflow is the most effective way to move gas from the disc to the inner regions, and numerical simulations have shown that once the central mass becomes too large the bar is subsequently destroyed (Hasan & Norman 1990). Thus, if a bar was originally responsible for fuelling the AGN and star formation, we do not necessarily expect to observe it at the current epoch. Although bars are able to transport gas from the disc to the ILR, there remains the problem of driving it further in to fuel the AGN. A small-scale inner bar, as is seen in NGC 7552 (Forbes, Katilainen & Moorwood 1994), may overcome this difficulty, but no corresponding feature is apparent in Circinus. Forbes et al. speculated that the nucleus in NGC 7552 may eventually become active as the inner bar drives gas to the nucleus; in Circinus it is possible that the opposite is occurring, and once its current supply of fuel is exhausted the AGN may switch to a dormant phase.

3.3 [Fe II] 1.64 μm

There are two competing mechanisms for [Fe II] emission in composite galaxies (those which host a Seyfert nucleus as well as a circumnuclear starburst). Near star-forming regions, the dominant process is shock excitation in SNRs where the iron gas-phase abundance is thought to be enhanced by grain destruction behind fast shocks. In a partially ionized zone around an AGN it can also be efficiently photoionized by a power-law continuum (e.g. Mouri et al. 1990; Simpson et al. 1996). Determining the relative contributions is an important step toward understanding such galaxies.

The [Fe II] morphology in Fig. 1(b) is rather different to that of the H_2. Although there is still a prominent peak associated with the AGN, a ridge that is not apparent on the [Fe II] line maps of Moorwood & Oliva (1994) extends about 2 arcsec to the north. From this image it is not clear whether this is a single elongated structure or two separate peaks which appear to merge due to the 1.4-arcsec resolution. However, in the higher resolution images of Marconi et al. (1994) the emission is clearly resolved into two peaks at 5000 Å. Marconi et al. also observed faint peaks of Hα and [S II] in the same region, indicative of H II regions or SNRs. We therefore interpret the extended emission as two distinct features. Our detection of [Fe II] in the northern peak is consistent with SNRs, and could in principle be produced by a single SNR. The [Fe II] 1.64-μm luminosity of the northern source is $L_{[\mathrm{Fe\,II}]}(\mathrm{W}) = 30.7$, lying between the estimated luminosities for young ($\lesssim 100$ yr) and evolved ($\sim 10^4$ yr) remnants, for which $\log L_{[\mathrm{Fe\,II}]}(\mathrm{W}) \approx 32$ and 30 respectively (Greenhouse et al. 1991; Lumsden & Puxley 1995). We may ask whether this is consistent with the lack of any associated peak in the H_2 or continuum emission. H_2 emission will only occur if the shock is driving into a molecular cloud; even assuming this to be so, we expect very little H_2 emission in a young SNR, since Draine, Roberge & Dal-

garno (1983) and Burton et al. (1990) have found that in SNRs the maximum efficiency for 1–0S(1) emission is attained when the shock speed is $v \lesssim 50$ km s^{-1}, which (assuming Sedov expansion) is only reached after $\sim 10^4$ yr. Furthermore, a single SNR would not produce significant *H*- or *K*-band continuum emission.

The extended emission, also probably generated by SNRs, is rather non-uniform, in contrast to the H_2 emission. The clumpy nature of the [Fe II] emission could be due to a relatively small number of individual SNRs, or it may be from diffuse emission at a level just below our 2.5σ threshold. On these grounds we can only limit the number of remnants we have observed in a 30×30 arcsec^2 aperture to less than about 50, simply by dividing the luminosity in the line by the typical luminosity of an evolved SNR. However, although the galaxy is one of the closest Seyfert 2 galaxies, the size of even evolved remnants ($\lesssim$15 pc; Lumsden & Puxley 1995) is consistent with their detection as unresolved sources. As such, the signal-to-noise ratio is sufficient for us to detect a single SNR with a luminosity of $\log L_{[\mathrm{Fe\,II}]}(\mathrm{W}) > 30$. The rather uneven morphology thus suggests that far fewer remnants, but brighter and hence younger ones, are seen. We infer from the detection of these supernova events that the star formation around the nucleus has either ended less than 10^8 yr ago, or is ongoing with a SN rate of 0.005 yr^{-1}, equivalent to a modest star formation rate of $< 1\ \mathrm{M}_\odot\ \mathrm{yr}^{-1}$ for a standard IMF. This SN rate is rather uncertain, since it depends critically on how much grain depletion occurs in the shocks and the resulting iron gas-phase abundance, neither of which is a well-known quantity, but the detection of [Fe II] can still be attributed to star formation activity. Since the molecular torus around an AGN may extend up to a few, or even a few tens of, parsecs (Krolik & Begelman 1988), the star formation we observe here may be associated with it. This is not a new idea, although much of the evidence for it has come from observations of the blue featureless continuum (FC) in Seyfert 2 galaxies (e.g. Fernandes 1994). Many of these appear to have a strong extra component (FC2) that cannot be explained in terms of the AGN which is itself obscured by the torus. Our observations of SNRs within 100 pc of the nucleus, much closer than the star-forming ring, appear to uphold this interpretation of the FC2.

Our failure to detect any significant [Fe II] emission in the ring at distances of about 10 arcsec from the nucleus cannot be explained by heavy extinction because of the strong Hα emission (Marconi et al. 1994). Since we expect to be able to detect a single evolved remnant, it indicates that there are no supernovae less than a few $\times 10^4$ yr old in this region. The typical time-scale for supernovae to appear following the onset of star formation is a few $\times 10^6$–10^7 yr (Leitherer & Heckman 1995), strongly suggesting that the star formation in the ring is in its early phases.

Forbes & Ward (1993) discuss [Fe II] emission by jet-induced shocks, and recent observations of the archetypal Seyfert 2 plus starburst NGC 1068 (Blietz et al. 1994) do show that the [Fe II] emission is enhanced along the nuclear radio jet. This has been attributed to grain destruction and shock or X-ray excitation at the outflow/cloud interface. By analogy we would expect to see similarly enhanced [Fe II] emission along the ionization cone and radio jets in Circinus. Although the [Fe II] is extended in other directions, *none* is observed along the ionization cone to the north-west. As the emission is extended in the other directions, this absence is particularly marked. If the H_2 emission traced only star formation, and SNRs in particular, we would expect it to follow the [Fe II] morphology reasonably closely. On the contrary, it *is* extended to the north-west, giving the overall morphology a more symmetrical appearance. A similar situation is seen in NGC 253 (Forbes et al. 1993), where there is wispy H_2 emission perpendicular to the major axis of the galaxy but no corresponding [Fe II]. Here we put forward three possibilities that might be able to account for this. First, Blietz et al. noted that the surface brightness of the emission in NGC 1068 decreased rapidly where the radio jet appeared to widen, and that there was some correspondence between the H_2 and radio emission, possibly hinting at some sort of collimation mechanism. We observe only weak extended H_2 emission in Circinus, so that the jet flaring may occur close to the nucleus and the [Fe II] emission quickly becomes too weak to detect. An alternative is a density effect. H_2 can be shock-excited over a wide range of densities, and is often modelled for 10^3–10^6 cm^{-3} (e.g. Burton et al. 1990), whereas the critical density for the $^4\mathrm{D}_{7/2}$ state of Fe is $\sim 2 \times 10^5$ cm^{-3} and so the [Fe II] lines only probe densities close to this. A low density of 10^2–10^3 cm^{-3} would account for the lack of [Fe II], an argument propounded by Forbes et al. (1993) for the regions of extended H_2 in NGC 253. The third possibility concerns the shock speed. The iron gas-phase abundance is enhanced by shocks only if the shock speed is high enough to destroy the grains, i.e. $v \gtrsim 100$ km s^{-1}. If instead the shock speed were significantly lower, $v \lesssim 50$ km s^{-1}, the efficiency of H_2 cooling would increase and the 1–0S(1) line would be observed in place of [Fe II].

3.4 Radio continuum

Maps of the radio continuum at 3 and 6 cm are shown in Fig. 3. These observations are insensitive to emission more extended than that shown here. The higher resolution 3-cm map partially resolves the central source and, after quadrature correction for the beamsize, we estimate its size as 0.8×0.5 arcsec^2. The flux from this source is 34 mJy, found by fitting a Gaussian to the nuclear emission. The spectral index, measured in a 1-arcsec aperture after smoothing the 3-cm map to the same resolution as the 6-cm map, is $\alpha = 0.1$ ($F_\nu \propto \nu^{-\alpha}$). These measurements are summarized in Table 2. Heisler & Norris (1997, in preparation) have shown that there is a weak (18 mJy at 13 cm) AGN core in the nucleus. The higher flux density measured here (after correction for spectral index) indicates that the AGN is accompanied by extended emission. In principle, a flat radio spectral index could be associated with free–free emission in H II regions, but Condon, Huang & Yin (1991) argue that even in *IRAS* ultraluminous galaxies this is unlikely to be a significant contributor to the radio flux. An alternative is that we are seeing synchrotron self-absorption, which produces the flat-spectrum ($\alpha \lesssim 0.5$) AGN cores in quasars and radio-loud galaxies. However, like most of the flat-spectrum sources observed by Condon et al., the 3-cm radio core in Circinus is extended, suggesting that the brightness temperature is too low for this to be important. On the other hand, it is possible that the flat spectrum is due to free–free absorp-

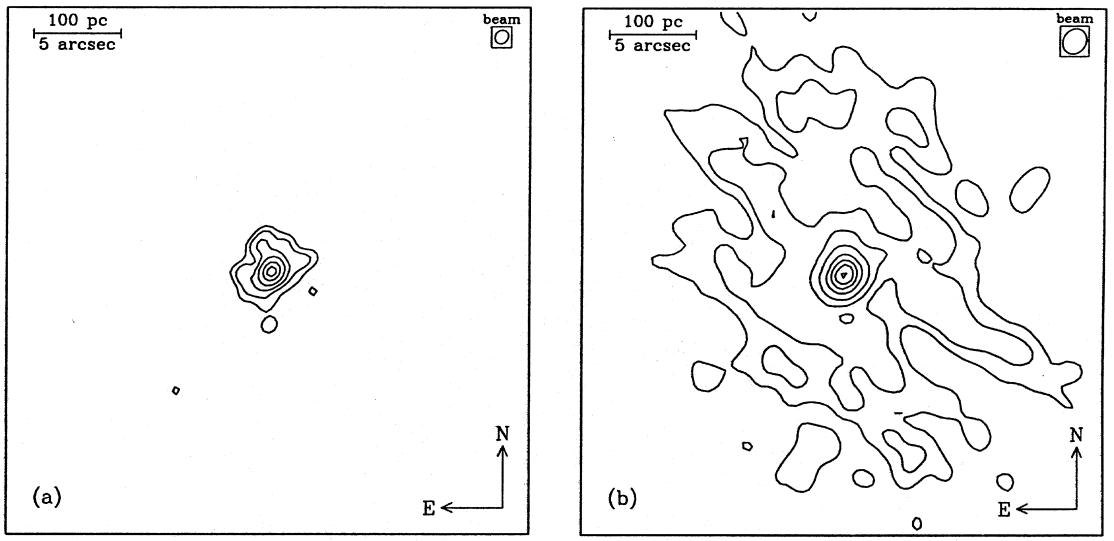

Figure 3. Radio continuum maps. (a) At 3 cm with a beam 1.06×0.91 arcsec^2 oriented at PA $= -39°$; contour levels are 1, 2, 4, 8, 16 and 24 mJy beam^{-1}. (b) At 6 cm with a beam 1.92×1.64 arcsec^2 oriented at PA $= -35°$; contour levels are 1, 2, 4, 8, 16, 24, 32 and 40 mJy beam^{-1}.

Table 2. Radio continuum.

Region/Feature	Flux Density (mJy) 3 cm	6 cm	Spectral Index
1 arcsec[a]	6.5	7.2	0.1
2 arcsec[a]	20.4	20.5	0.0
Nucleus[b]	34	—	—
Northern peak[b]	5	—	—

[a]Diameter of aperture used; 3-cm map smoothed to resolution of 6-cm map.
[b]Estimated by fitting Gaussians; see text for details.

tion of optically thin synchrotron radiation (from supernovae or an AGN), indicating intense star formation. A fuller discussion of the radio mechanisms will be given in Forbes & Norris (1997, in preparation); here we simply note that the size and flux density of the nucleus at 3 cm is consistent with a free–free opacity $\tau_{ff} = 1$ at $\nu =$ a few GHz (Condon et al. 1991), implying that free–free absorption could be an important process. In this case the H_2 and [Fe II] emission are more likely to be from star formation at relatively low optical depth than from the AGN. Forbes & Ward (1993) found a correlation between the 6-cm radio continuum and [Fe II] line flux for starburst and Seyfert galaxies. The nuclear emission from Circinus fits this correlation well at the lower luminosity end.

The 3-cm map clearly shows other features within a few arcsec of the nucleus. The most prominent of these is an unresolved source which lies 1.6 arcsec away at a PA of 22°, a position virtually the same as that of the northern [Fe II] peak. Since the separation of the centroid of this region from the nucleus is more than three times the half-width of the beam, we surmise that it is not a result of the finite beamsize but a distinct feature. We estimate the flux in this source to be 5 mJy, but cannot measure its spectral index due to the poorer resolution of the 6-cm map. If we scale the flux to 5 GHz (using the canonical spectral index $\alpha = 0.8$; Condon & Yin 1990) at the distance of the starburst galaxy M82 (3.2 Mpc), we calculate a flux of 13 mJy, similar to the brightest SNRs observed by Muxlow et al. (1994) in that galaxy. They measured remnants this bright to have sizes of about 1 pc and estimated their ages to be ~ 200 yr, a value consistant with our previous hypothesis that the [Fe II] emission was from a single remnant that was too young, and hence still had shock speeds too high to produce observable H_2 emission.

There remain two weaker features apparent in the 3-cm map at the 3–3.5 mJy beam^{-1} level, diametrically opposite each other, 3.3 arcsec apart at PAs of $-77°$ and 103°. The beamsize of the 6-cm map is larger by nearly a factor of 2, and only a hint of the north-west feature is apparent in the 4 mJy beam^{-1} contour. These may be the inner parts of the jet which form the lobes seen by Harnett et al. (1990) and Elmouttie et al. (1995) that extend over 1 arcmin from the nucleus; it is interesting to note that the PAs of these lobes are reported as $-66°$ and 114°, and $-45°$ and 115° respectively. A simple calculation shows that the maximum radio continuum intensity observed in the lobes at 13 and 20 cm by Elmouttie et al. yields, using a spectral index of 0.7 close to the measured range of 0.6–0.7, a 6-cm flux density of 0.6 mJy beam^{-1} which is below our detection threshold and can explain why we do not detect extended emission in the jets.

We have detected emission 10 arcsec to the north of the AGN at 6 cm which could be associated with the star-forming ring, but since it is below the detection threshold at 3 cm we are only able to put a lower limit on the spectral index. In the 6-cm map the peak flux density to the north in the ring is 2 mJy beam^{-1}, whereas in the 3-cm map it is < 1 mJy beam^{-1}. Since the 6-cm beam is much larger, the spectral index is $\alpha < 0.7$, consistent with both free–free emission from H II regions and synchrotron radiation from SNRs. The radio emission therefore does not contradict our conclusion that the star formation in the ring is very young.

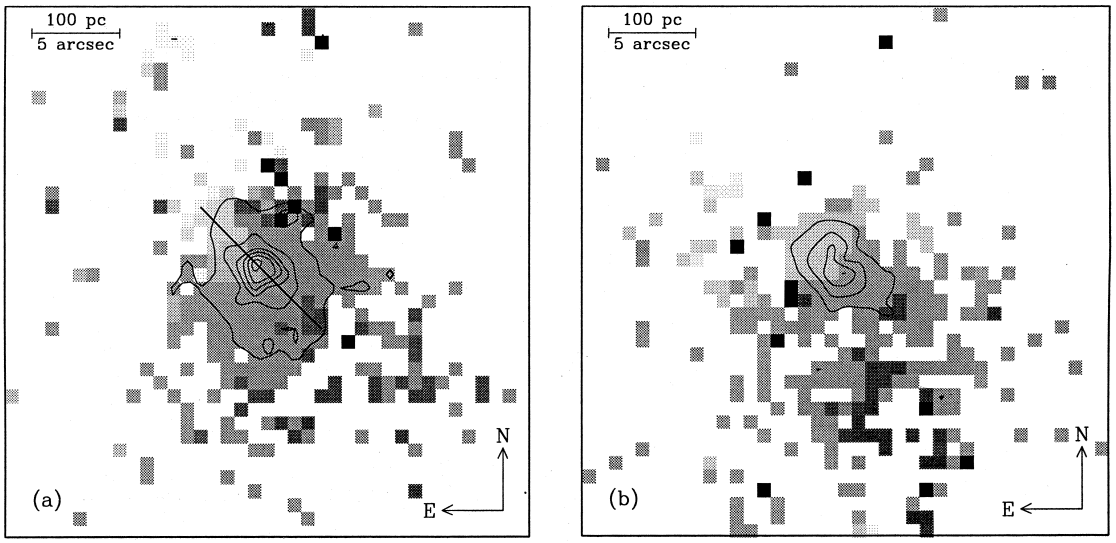

Figure 4. Velocity maps (grey-scale) for high signal-to-noise ratio pixels in the central 30×30 arcsec^2; intensity contours are superimposed. Light regions indicate velocities towards the observer, and dark regions recession. (a) H_2 1–0S(1) 2.12 μm. The velocities are shown over ~ 400 km s^{-1}, and contours are at every 1.6×10^{-18} W m^{-2} arcsec^{-2}. The solid line indicates the vector along which velocities shown in Fig. 5 were extracted. (b) [Fe II] 1.64 μm. The velocity range shown covers ~ 300 km s^{-1}, and contours are at every 2×10^{-18} W m^{-2} arcsec^{-2}.

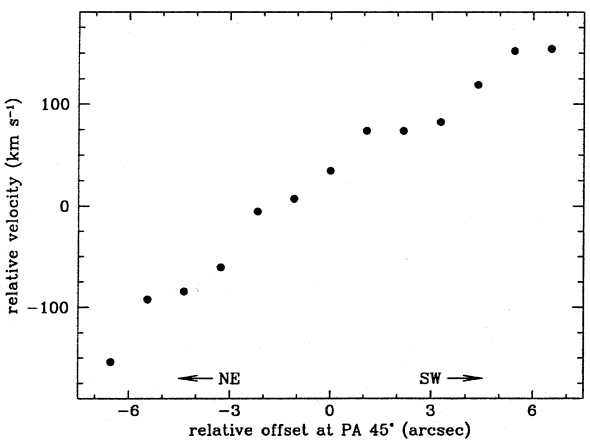

Figure 5. Velocity slice extracted from the H_2 velocity map. The slice, indicated by the solid line in Fig. 4(a), is a single pixel wide and crosses the centre at PA = 45° with negative offsets towards the north-east.

Other source visible in the lowest contour of the 3-cm map to the south of the nucleus may be associated with the extended [Fe II] emission. However, as these features are very weak, it is not possible to discuss them in detail.

3.5 Velocity maps

Fig. 4 shows relative velocity maps for H_2 and [Fe II], including only the highest signal-to-noise ratio pixels. The maps for both emission lines are broadly consistent, the only clear feature being a gradual increase in velocity from north to south along a PA of 30°–50°, the galaxy's major axis, indicating pure galaxy rotation. We have plotted in Fig. 5 a slice from the H_2 velocity map, 1 pixel wide and extracted across the centre at PA = 45°. It shows clearly that the velocity gradient is linear with position and has a scale on the order of 300 km s^{-1} along 14 arcsec, consistent with measurements of radio emission by other authors. Freeman et al. (1977) observed a maximum velocity of ± 137 km s^{-1} along the same PA, and using a 12.5-arcmin beam Harnett et al. (1990) reported a velocity spread in OH absorption of 180 km s^{-1}. Our velocity maps are at a much higher spatial resolution and, though not really adequate to determine rotation curves, appear to be consistent with solid body rotation through the inner regions. Measurements of the circumnuclear region of both lines yields ± 40 km s^{-1} within ± 1.4–2.1 arcsec, which can be corrected for inclination to give an upper limit to the central mass. The derived mass of $(1–2) \times 10^7$ $M_\odot$ is within the range of black hole masses ($\sim 3 \times 10^6$ to $\sim 5 \times 10^8$ $M_\odot$; Blandford 1990) in the literature.

4 CONCLUSIONS

We have presented near-infrared images and velocity maps of the [Fe II] 1.64-μm and H_2 2.12-μm lines in the central regions of the Circinus galaxy, and radio continuum maps at 3 and 6 cm.

Both lines show prominent peaks (FWHM ~ 2 arcsec) at the nucleus, clearly separate from the circumnuclear emission. As these appear to be associated with the AGN, it may be that the [Fe II] arises in a partially ionized zone around it, and the H_2 is excited by X-ray irradiation of the molecular torus. However, since at 5 GHz the nucleus is resolved and has a flat spectral index (possibly due to free–free absorption of optically thin synchrotron radiation from supernovae or an AGN), we conclude that the AGN is very highly obscured and that the observable emission is more likely to be from a cluster of stars close to it.

Unlike NGC 1068, we do not see [Fe II] emission enhanced along the radio jet axis; on the other hand, the H_2 is extended in this direction. Possible reasons for this difference include slower shock speeds induced by the jet resulting in a lower iron gas-phase abundance and higher H_2 cooling efficiency, or a low-density environment which does not favour [Fe II] emission. The radio continuum shows only features close to the nucleus which could be the beginnings of jets; this suggests that any emission aligned with the jet may, like the radio emission, be below our detection threshold.

Previous Hα line imaging revealed star formation occurring in a ring, particularly to the north of the nucleus. At a signal-to-noise ratio high enough to detect individual SNRs we have failed to observe any significant [Fe II] emission in this ring, constraining the age of the star formation to less than a few $\times 10^7$ yr. This conclusion is not contradicted by the radio continuum emission. The H_2 distribution (decreasing towards the ring) implies that the star formation cannot have progressed outward from the AGN, and that it is probably only related to it because they share the same fuelling mechanism that drives disc gas inwards.

We have detected clumpy [Fe II] emission within 100 pc around the nucleus, which we attribute to SNRs less than 10^4 yr old. An extension to the north is consistent with a point source 2 arcsec (40 pc) from the nucleus, and could be due to a single remnant. We also detect this source in the radio continuum, but not in the H_2 lines or near-infrared continuum, results which are all consistent with a young (a few hundred year old) supernova remnant. Most previous evidence for star formation in the tori of AGN has been based on an extra component to the blue featureless continuum that is seen in many Seyfert 2 galaxies. Our results are direct evidence that star formation occurs in and around the molecular torus.

Velocity maps of both lines show a velocity gradient along the major axis of the galaxy, consistent with simple rotation. We estimate the mass within the central 30 pc to be on the order of 10^7 $M_\odot$.

These results suggest that further high signal-to-noise and high spatial resolution studies are warranted, in order to investigate the AGN and star formation in both the torus and circumnuclear ring, and to clarify the issue concerning radio emission along the jets and the associated jet-induced H_2 emission.

ACKNOWLEDGMENTS

We thank the anonymous referee for comments which have helped to improve this paper. RID acknowledges the support of a PPARC (EPSRC) research studentship grant.

REFERENCES

Allen D. A. et al., 1993, Proc. Astron. Soc. Aust., 10, 298
Blandford R. D., 1990, in Courvoisier T., Mayor M., eds, Active Galactic Nuclei. Saas-Fee Advanced Course 20, Springer-Verlag, Berlin
Blietz M., Cameron M., Drapatz S., Genzel R., Krabbe A., van der Werf P., Sternberg A., Ward M., 1994, ApJ, 421, 92
Burton M. G., Hollenbach D. J., Haas M. R., Erickson E. F., 1990, ApJ, 355, 197
Condon J. J., Yin Q. F., 1990, ApJ, 357, 97
Condon J. J., Huang Z.-P., Yin Q. F., 1991, ApJ, 378, 65
Draine B. T., Roberge W. G., Dalgarno A., 1983, ApJ, 264, 485
Elmouttie M., Haynes R. F., Jones K. L., Ehle M., Beck R., Wielebinski R., 1995, MNRAS, 275, L53
Fernandes R. C., 1994, in Ward M. J., ed., Proceedings of the Oxford Torus Workshop
Forbes D. A., Ward M. J., 1993, ApJ, 416, 150
Forbes D. A., Ward M. J., Rotaciuc V., Blietz M., Genzel R., Drapatz S., Vander Werf P., Krabbe A., 1993, ApJ, 406, L11
Forbes D. A., Kotilainen J. K., Moorwood A. F. M., 1994, ApJ, 433, L13
Freeman K. C., Karlsson B., Lynga G., Burrell J. F., van Woerden H., Gross W. M., Mebold U., 1977, A&A, 55, 445
Gardner F. F., Whiteoak J. B., 1982, MNRAS, 201, 13P
Greenhill L., Ellingsen S., Norris R., Gough R., Sinclair M., Moran J., Mushotsky R., 1997, ApJ, 474, L103
Greenhouse M., Woodward C., Thronson H., Rudy R., Rossano G., Erwin P., Puetter R., 1991, ApJ, 383, 164
Harnett J. I., Whiteoak J. B., Reynolds J. E., Gardner F. F., Tzioumis A., 1990, MNRAS, 244, 130
Hasan H., Norman C., 1990, ApJ, 361, 69
Howarth I. D., 1983, MNRAS, 203, 301
Krolik J. H., Begelman M. C., 1988, ApJ, 329, 702
Leitherer C., Heckman T. M., 1995, ApJS, 96, 9
Lepp S., McCray R., 1983, ApJ, 269, 560
Lumsden S., Puxley P. J., 1995, MNRAS, 276, 723
Marconi A., Moorwood A. F. M., Origlia L., Oliva E., 1994, Messenger, 78, 20
Matt G. et al., 1996, MNRAS, 81, L69
Moorwood A. F. M., Glass I. S., 1984, A&A, 135, 281
Moorwood A. F. M., Oliva E., 1988, A&A, 203, 278
Moorwood A. F. M., Oliva E., 1994, Infrared Phys. Technol., 35, 349
Moorwood A. F. M., Lutz D., Oliva E., Marconi A., Netzer H., Genzel R., Sturm E., de Graauw T., 1996, A&A, 315, L109
Mouri H., Nishida M., Taniguchi Y., Kawara K., 1990, ApJ, 360, 55
Muxlow T. W. B., Pedlar A., Wilkinson P. N., Axon D. J., Sanders E. M., de Bruyn A. G., 1994, MNRAS, 266, 455
Oliva E., Salvati M., Moorwood A. F. M., Marconi M., 1994, A&A, 288, 457
Pfenniger D., Norman C., 1990, ApJ, 363, 391
Puxley P. J., Hawarden T. G., Mountain C. M., 1990, ApJ, 364, 77
Simpson C., Forbes D. A., Baker A. C., Ward M. J., 1996, MNRAS, 283, 777
Whiteoak J. B., Gardner F. F., 1986, MNRAS, 222, 513
Yi I., Field G. B., Blackman E. G., 1994, ApJ, 432, L31